

PREPARED FOR SUBMISSION TO JHEP

Baryon-number - flavor separation in the topological expansion of QCD

David Frenklakh^a, Dmitri Kharzeev^{a,b}, Giancarlo Rossi^{c,d} and Gabriele Veneziano^{e,f}

^aCenter for Nuclear Theory, Department of Physics and Astronomy, Stony Brook University, Stony Brook, NY 11974-3800, USA

^bDepartment of Physics, Brookhaven National Laboratory, Upton, NY 11973-5000, USA

^cDipartimento di Fisica, Università di Roma “Tor Vergata” INFN, Sezione di Roma “Tor Vergata”, via della Ricerca Scientifica - 00133 Roma, Italy

^dCentro Fermi - Museo Storico della Fisica e Centro Studi e Ricerche E. Fermi, via Panisperna 89a, 00184 Roma, Italy

^eTheory Department, CERN, CH-1211, Geneva 23, Switzerland

^fCollège de France, 11 place M. Berthelot, 75005 Paris, France

E-mail: david.frenklakh@stonybrook.edu,
dmitri.kharzeev@stonybrook.edu, rossig@roma2.infn.it,
gabriele.veneziano@cern.ch

ABSTRACT: Gauge invariance of QCD dictates the presence of string junctions in the wave functions of baryons [1]. In high-energy inclusive processes, these baryon junctions have been predicted to induce the separation of the flows of baryon number and flavor [2]. In this paper we describe this phenomenon using the analog-gas model of multiparticle production proposed long time ago by Feynman and Wilson [3] and adapted here to accommodate the topological expansion in QCD [4, 5]. In this framework, duality arguments suggest the existence of two degenerate junction-antijunction glueball Regge trajectories of opposite \mathcal{C} -parity with intercept close to $1/2$. The corresponding results for the energy and rapidity dependence of baryon stopping are in reasonably good agreement with recent experimental findings from STAR and ALICE experiments. We show that accounting for correlations between the fragmenting strings further improves agreement with the data, and outline additional experimental tests of our picture at the existing (RHIC, LHC, JLab) and future (EIC) facilities.

KEYWORDS: $1/N$ Expansion, Specific QCD Phenomenology, Hadron-Hadron Scattering, Properties of Hadrons

Contents

1	Introduction	2
2	The planar Feynman-Wilson gas (FWG) and the Reggeon intercept	5
3	FWG at the cylinder level	6
3.1	The Pomeron Intercept	7
4	Feynman-Wilson gas with baryons	8
4.1	FWG for baryon-antibaryon annihilation	8
5	Regge trajectories and spectra of the junction-antijunction glueballs	11
6	Transport of flavor and baryon number	14
6.1	Quark/flavor transport in meson-meson scattering	15
6.2	Baryon and flavor transport in meson-baryon scattering	17
6.3	Baryon and flavor transport in baryon-(anti)baryon scattering	18
6.4	Combined charge–baryon-number rapidity distribution	19
6.5	Rapidity distribution of $B\bar{B}$ -pair creation	21
7	Predictions and experimental tests	22
A	Derivation of equation (2.2)	24

1 Introduction

In QCD the wave functions of asymptotic states (hadrons) have to be gauge-invariant. For a meson composed by a quark located at point x_2 and an antiquark at point x_1 , the gauge invariance can be enforced by introducing the path-ordered exponential operator

$$U(\mathcal{C}(x_1, x_2)) \equiv P \exp \left(ig \int_{\mathcal{C}(x_1, x_2)} A_\mu(x) dx^\mu \right) \quad (1.1)$$

constructed from the gluon field $A_\mu \equiv t^a A_\mu^a$, yielding the meson wave function

$$M(\mathcal{C}(x_1, x_2)) = \bar{q}(x_1) U(\mathcal{C}(x_1, x_2)) q(x_2). \quad (1.2)$$

Here \mathcal{C} denotes a path going from x_1 to x_2 . For baryons, the unique way to construct a gauge-invariant wave function is to join three string operators at a junction, as proposed in [1]:

$$B(\mathcal{C}_1, \mathcal{C}_2, \mathcal{C}_3) = \epsilon^{ijk} [U(\mathcal{C}_1(x, x_1))q(x_1)]_i [U(\mathcal{C}_2(x, x_2))q(x_2)]_j [U(\mathcal{C}_3(x, x_3))q(x_3)]_k. \quad (1.3)$$

The string operator $U(\mathcal{C}(x, x_n))$ acting on a quark field located at space-time point x_n makes it transform under gauge transformations as a field at point x . The antisymmetric tensor then makes a color-singlet and gauge-invariant state out of the three quarks plus the junction.

At strong coupling, the string operators describe strings connecting the quarks to a common “baryon junction”, which thus becomes, along with the three quarks, a fourth constituent of the baryon [1]^{1,2}. Baryonic (anti)junctions (\bar{J}) J give rise to new exotic hadrons, including baryonium-like $J - \bar{J}$ states with additional two, one, or no $q - \bar{q}$ constituent quark-antiquark pairs, penta-quarks, dibaryons, and other exotics [1, 9]. It was stressed in [1] (see also [7]) that duality diagrams involving baryons and anti-baryons are ambiguous unless the flow of the junction, indicating the flow of baryon number, is shown together with the flow of flavor associated with the valence quarks. Regge trajectories containing $J - \bar{J}$ states provide new contributions to high-energy amplitudes of exclusive processes involving baryons and antibaryons [1, 9].

In high energy inclusive processes involving baryons, the existence of junctions was predicted to lead to the separation of flows of baryon number and flavor [2]³. The origin of this phenomenon is easy to understand. At strong coupling, the string operators in (1.3) describe strings inside the baryon. In high energy baryon collisions, the valence quarks that carry large Bjorken momentum fraction x end up in the fragmentation region of the

¹We should stress that in such a constituent-parton picture the junction itself is in a non-trivial color representation such as to compensate for the one of the three valence quark system.

²For heavy/static quarks the junction naturally emerges also in the context of the AdS/CFT correspondence [6] and in lattice QCD at strong coupling [7]. Its appearance at the so-called Fermat-Torricelli point has been nicely confirmed by lattice-QCD calculations [8].

³This phenomenon is somewhat analogous to the spin-charge separation in condensed matter physics (see e.g. [10]), which also has a topological origin.

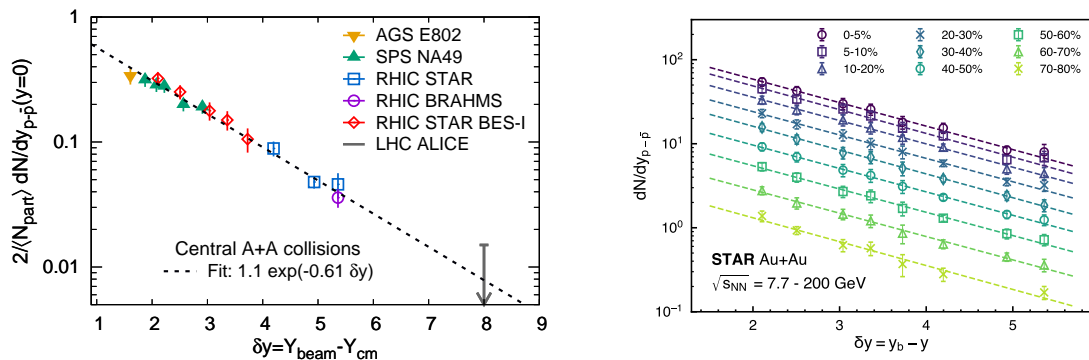


Figure 1. Left panel: compilation of data from various experiments on the rapidity slope parameter that is related to the intercept of J_0 trajectory by the means of Eq. (1.4). Right panel: rapidity distribution of baryons from the Beam Energy Scan at RHIC. Evidently, the slope is almost independent of centrality in agreement with baryons stopping mediated by J_0 exchange. The centrality-averaged fit to the slope is about 0.65 ± 0.1 [13]. In both panels $\delta y = Y/2$ is the beam rapidity in c.m.s. Both figures are reproduced from [13] with kind permission of The European Physical Journal (EPJ).

process, but the gluonic junction can be more easily stopped in the central rapidity region. The strings that connect the junction to the valence quarks then break by producing additional quark-antiquark pairs, but the baryon is always reconstructed around the junction. Its valence quark content is however not correlated with the one of the original baryon participating in the collision – so the flows of baryon number and flavor are uncorrelated and separated in rapidity. The computation of inclusive baryon stopping cross section was performed in [2] within the Mueller-Kancheli generalized optical theorem approach [11, 12], using for the intercept of the leading junction-antijunction quarkless J_0 trajectory the value $\alpha_{J_0} = 0.5$ originally proposed in [1]. The produced baryons are distributed in the c.m.s. rapidity y_f according to [2]:

$$\frac{dN}{dy_f} \propto e^{(\alpha_{J_0} + \alpha_{\mathbb{P}} - 2)Y/2} [e^{(\alpha_{\mathbb{P}} - \alpha_{J_0})y_f} + e^{(\alpha_{J_0} - \alpha_{\mathbb{P}})y_f}], \quad (1.4)$$

where Y is the rapidity separation between the beams.

Recently baryon stopping was studied at RHIC in AA and γA (through ultraperipheral processes) collisions [13]. The beam rapidity dependence of the number of stopped baryons is shown in Fig. (1), reproduced from [13]. In Eq. (1.4) the slope of the beam rapidity dependence is given by $(\alpha_{J_0} + \alpha_{\mathbb{P}} - 2) = (\alpha_{J_0} + \Delta - 1)$ where we used $\Delta = \alpha_{\mathbb{P}} - 1 \simeq 0.08$, as fixed by the “soft” Pomeron intercept $\alpha_{\mathbb{P}} \simeq 1.08$ [14]. If one uses the value of $\alpha_{J_0} \simeq 0.5$, as originally suggested in [1], the beam rapidity dependence becomes $e^{-0.42 Y/2}$, to be contrasted with $e^{-0.65 Y/2}$ from the Beam Energy Scan at RHIC, see the right panel of Fig. (1). Thus, the agreement between the data and the prediction made with the original value of α_{J_0} is reasonable. However, with the increased precision of the data it is necessary to revisit the prediction for the α_{J_0} intercept. This is what we attempt to do in this paper.

Because the processes of baryon stopping are dominated by small or moderate momentum transfer, they have to be described in the strong coupling domain where the topological expansion of QCD [4, 15] can be used as a guiding principle. It is important to develop an approach to high-energy baryon interaction that combines known general features of inclusive processes with the properties of the topological expansion of QCD. For this purpose, it is useful to refer to an approach to high energy multi-hadron production processes proposed long time ago by Feynman and Wilson.

In the early seventies, after Feynman’s introduction of the concept of inclusive reactions [16] (see also [17]) and his rediscovery of the Amati-Fubini-Stanghellini scaling in the multiperipheral model [18] (see also [19]), Feynman himself and Ken Wilson ([3] and private communication cited therein) introduced an interesting analog model of multiparticle interactions assimilating the generating function(al) of inclusive cross sections to the grand-canonical partition function of a gas in a finite volume.

One obstacle encountered in the Feynman-Wilson-gas (FWG) formulation was to define and isolate the kind of inclusive cross section (including the simplest of them, the total cross section) to which the FWG formulation could be applied. In particular, Ref. [3] argues that diffractive processes (diffractive scattering and dissociation) should be taken out before defining the gas analog and its properties.

Large- N expansions, either in the context of the hadronic string or of QCD, can help precisely in formulating the FWG model on a much firmer theoretical basis. However, since multiparticle production is an essential element of the FWG model, the large- N_c expansion by ’t Hooft [20], in which quark loops are suppressed, cannot be used. Rather, one can appeal to the topological expansion (TE) formulated by one of us, either in the context of the dual resonance model [4] or, even better, of QCD [5], where the large- N limit is taken at fixed N_f/N_c . Also instrumental for justifying some assumptions is the use of the Mueller-Kancheli approach [11, 12] to compute the high-energy behavior of inclusive cross sections through appropriately generalized optical theorems.

The plan of the paper is as follows. In Section 2 we concentrate our attention on the planar approximation and its non-linear, exact bootstrap constraints, obtaining a relation between the $q\bar{q}$ leading Reggeon intercept and the “pressure” of a one-species FWG. In Section 3 we turn our attention to the cylinder topology which is supposed to describe the bare soft Pomeron appearing at the next to leading order in the TE. Its description is in terms of a two-species FWG. We are thus able to connect the distance of the Pomeron intercept $\alpha_{\mathbb{P}}$ from 1 to the cross correlations between the two species. In Section 4 we move to the case of $B\bar{B}$ annihilation into mesons which is suitably described in terms of a three-species FWG. We provide estimates of the intercepts of Regge trajectories corresponding to mesons with a junction-antijunction pair that control different inclusive annihilation cross sections. In Section 5 we use the estimated J_0 Regge trajectory to predict the spectrum of J_0 glueballs that can be looked for in lattice QCD calculations and we propose an expression of the glueball operator that can be used for that purpose. Section 6 discusses the main observable consequences of our framework: it deals first, separately, with

flavor and baryon-number transport in various processes (meson-meson, meson-baryon, baryon-baryon, baryon-antibaryon scattering), it then extends the treatment to the combined flavor–baryon-number rapidity distribution, and finally ends with a discussion of the inclusive distribution of $B\bar{B}$ pair production, as a function of their relative rapidity. In Section 7 we propose several independent experimental tests to further examine the role of baryon junctions in high-energy processes. In Appendix A we outline (our understanding of) the FWG model in the case of inclusive cross sections as functions of rapidity (i.e. after having integrated over the transverse phase space).

2 The planar Feynman-Wilson gas (FWG) and the Reggeon intercept

In the planar limit for meson-meson scattering the FWG model consists of just one species of mesons for which one can define the grand-canonical partition function

$$\Sigma_{pl}(z) = \frac{1}{\sigma_t^{pl}} \sum_{n \geq 2} z^n \sigma_n^{pl} \quad \Rightarrow \quad \Sigma_{pl}(1) = 1 \quad (2.1)$$

where we have normalized the individual exclusive cross sections σ_n^{pl} to the total planar cross section σ_t^{pl} and we omitted to indicate that all these quantities depend on the center-of-mass energy \sqrt{s} . Assuming short-range correlations we may also write (see Appendix A):

$$\begin{aligned} \Sigma_{pl}(z) &\equiv \exp(Yp(z)) = \exp\left(Y \sum_{m \geq 1} c_m \frac{(z-1)^m}{m!}\right) ; \\ p(1) &= 0, \quad p'(1)Y = c_1 Y = \langle n \rangle, \quad p''(1)Y = c_2 Y = \langle n(n-1) \rangle - \langle n \rangle^2, \\ p'''(1)Y &= c_3 Y = \langle n(n-1)(n-2) \rangle - \langle n \rangle^3 - 3c_1 c_2 Y^2, \\ p''''(1)Y &= c_4 Y = \langle n(n-1)(n-2)(n-3) \rangle - \langle n \rangle^4 - 6c_1^2 c_2 Y^3 - 4c_1 c_3 Y^2 - 3c_2^2 Y^2, \dots \end{aligned} \quad (2.2)$$

where $p(z)$ plays the role of the pressure⁴, as a function of fugacity z , and $Y \sim \log(s/p_\perp^2)$ is the rapidity (i.e. after having integrated over the transverse momenta, assumed to be strongly cut-off) “volume” occupied by the gas. It is a crucial fact, implied by Regge-pole factorization/dominance, that in (2.1) a single power of Y can be factored out, which corresponds to the assumption of short range correlations.

From standard Regge-pole dominance at high energy (see Table 1), and from the planar optical theorem (see Fig. (2)), it follows that, as $z \rightarrow 0$:

$$\Sigma_{pl}(z) \rightarrow \frac{\sigma^{pl}_{excl}}{\sigma_t^{pl}} \sim s^{\alpha_{\mathbb{R}}-1} \Rightarrow -p(0) = 1 - \alpha_{\mathbb{R}}(0) = \sum_m c_m \frac{(-1)^{m+1}}{m!} = \frac{\langle n \rangle}{Y} - \frac{c_2}{2} + \dots \quad (2.3)$$

This planar bootstrap result connects the Reggeon intercept to multiparticle correlations. In the case of vanishing correlations (i.e. of a Poisson distribution) one recovers a very old

⁴As explained in Appendix A, $p(z)$ is insensitive to any Y -independent prefactor needed to make Σ approach a finite limit as $z \rightarrow 0$. Also, we will only be interested in pressure differences which do not depend on the overall normalization of Σ_{pl} . This is why our pressure goes to zero at $z = 1$ while in a real gas it would make more sense to have it vanish at $z = 0$.

MM -planar	MM -cylinder	$B\bar{B}$ -annihilation
$\sigma_{excl}^{pl} \sim s^{2\alpha_{\mathbb{R}}-2}$		$\sigma_{excl}^{ann} \sim s^{2\alpha_{\mathbb{B}}-2}$
	$\sigma^{cyl}(n, 0) \sim s^{\alpha_{\mathbb{R}}-1}$	$\sigma^{ann}(n_1, 0, 0) \sim s^{\alpha_{\mathbb{J}_4}-1}$
		$\sigma^{ann}(n_1, n_2, 0) \sim s^{\alpha_{\mathbb{J}_2}-1}$
$\sigma_t^{pl} \sim s^{\alpha_{\mathbb{R}}-1}$	$\sigma_t^{cyl} \sim s^{\alpha_{\mathbb{P}}-1}$	$\sigma_t^{ann} = \sigma^{ann}(n_1, n_2, n_3) \sim s^{\alpha_{\mathbb{J}_0}-1}$

Table 1. Leading Regge behavior of cross-sections in different processes.

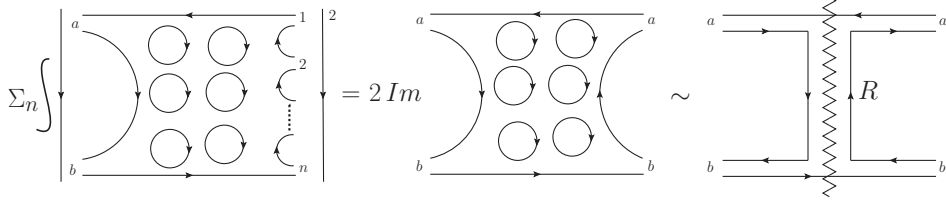


Figure 2. From left to right: optical theorem for the total planar cross section $\sum_X \sigma(a + b \rightarrow X)$ and its high-energy limit described by the leading $q\bar{q}$ Regge-pole exchange.

result by Chew and Pignotti [21] based on the simplest multiperipheral model, namely

$$\alpha_{\mathbb{R}}(0) = 1 - \frac{\langle n \rangle}{Y} \quad (2.4)$$

Hereafter, to simplify the notation, we will just indicate by α_i the intercept $\alpha_i(0)$ of a generic Regge trajectory.

3 FWG at the cylinder level

At the cylinder level the FWG consists of two species that we shall call “right” (R) and “left” (L) according to the picture in Fig. (3). We define accordingly:

$$\Sigma_{cyl}(z_R, z_L) = \frac{1}{\sigma_t^{cyl}} \sum_{n_R+n_L \geq 2} z_R^{n_R} z_L^{n_L} \sigma^{cyl}(n_R, n_L) \Rightarrow \Sigma_{cyl}(1, 1) = 1 \quad (3.1)$$

where we chose to normalize the individual exclusive cross-sections $\sigma^{cyl}(n_R, n_L)$ by the total cylinder cross-section σ_t^{cyl} . Assuming short-range correlations we now have, in place of (2.2):

$$\Sigma_{cyl}(z_R, z_L) \equiv \exp(Yp(z_R, z_L)) = \exp\left(Y \sum_{m_R+m_L \geq 1} c(m_R, m_L) \frac{(z_R-1)^{m_R} (z_L-1)^{m_L}}{m_R! m_L!}\right);$$

$$c(1,0)Y = \langle n_R \rangle, \quad c(0,1)Y = \langle n_L \rangle, \quad c(1,1)Y = \langle n_R n_L \rangle - \langle n_R \rangle \langle n_L \rangle, \quad \dots \quad (3.2)$$

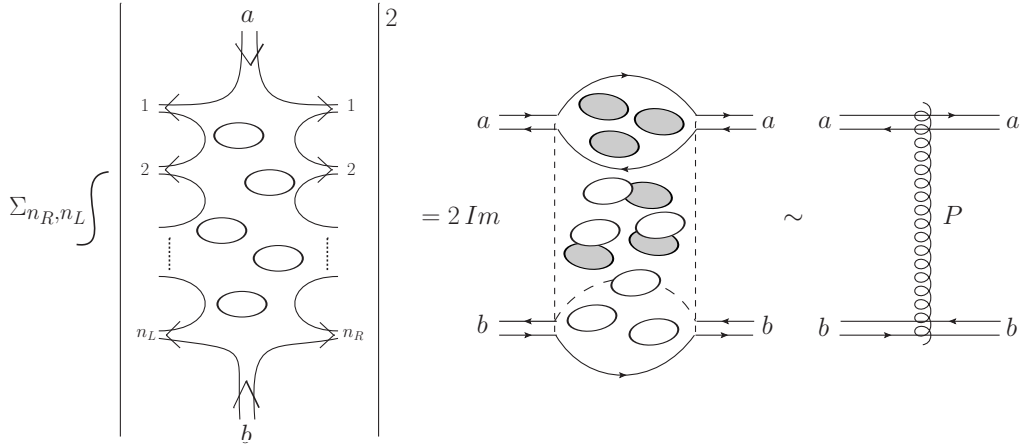


Figure 3. Total cylinder cross section seen as a two-species FWG and its high energy limit described by the (bare) Pomeron exchange.

It is convenient to separate out in (3.2) the terms with $n_R = 0$ and $n_L = 0$ and write:

$$\begin{aligned}
p(z_R, z_L) &= p_R(z_R) + p_L(z_L) + C_{RL}(z_R, z_L) \\
p_R(z_R) &= \sum_{m_R \geq 1} c(m_R, 0) \frac{(z_R - 1)^{m_R}}{m_R!}, \quad p_L(z_L) = \sum_{m_L \geq 1} c(m_L, 0) \frac{(z_L - 1)^{m_L}}{m_L!} \\
C_{RL}(z_R, z_L) &= \sum_{m_R, m_L \geq 1} c(m_R, m_L) \frac{(z_R - 1)^{m_R} (z_L - 1)^{m_L}}{m_R! m_L!}
\end{aligned} \tag{3.3}$$

One readily finds

$$p(1, 1) = p_R(1) = p_L(1) = C_{RL}(1, z_L) = C_{RL}(z_R, 1) = 0. \tag{3.4}$$

3.1 The Pomeron Intercept

In order to express the (bare)-Pomeron intercept $\alpha_{\mathbb{P}}$ in terms of the Reggeon intercept $\alpha_{\mathbb{R}}$ and the above correlators we note that

$$p(1, 0) + p(0, 1) - p(0, 0) + C_{RL}(0, 0) = 0, \tag{3.5}$$

where we have used the equations (3.3) as well as the relations in (3.4). On the other hand, recalling the results summarized in Table 1, we have $p(1, 0) = p(0, 1) = \alpha_{\mathbb{R}} - \alpha_{\mathbb{P}}$ while $p(0, 0) = 2\alpha_{\mathbb{R}} - 1 - \alpha_{\mathbb{P}}$. Inserting these values in (3.5) gives

$$\begin{aligned}
0 &= 2(\alpha_{\mathbb{R}} - \alpha_{\mathbb{P}}) - (2\alpha_{\mathbb{R}} - 1 - \alpha_{\mathbb{P}}) + C_{RL}(0, 0), \quad \text{i.e.} \\
\alpha_{\mathbb{P}} &= 1 + C_{RL}(0, 0) = 1 + \sum_{m_R, m_L \geq 1} \frac{c(m_R, m_L)}{m_R! m_L!} (-1)^{m_R + m_L} = 1 + \frac{\langle n_R n_L \rangle - \langle n_R \rangle \langle n_L \rangle}{Y} + \dots
\end{aligned} \tag{3.6}$$

The last equation reproduces the claim of [15] yielding a unit intercept for the (bare) Pomeron when $R - L$ correlations are negligible (so that the total pressure is the sum of

the pressures of the two species according to Dalton’s law)⁵ and extends it to the case in which they are not.

Comparing the Regge behavior of σ_{excl} , σ_t^{pl} and σ_t^{cyl} , we can say that $s^{\alpha_{\mathbb{R}} - \alpha_{\mathbb{P}}} = \exp(-Y(\alpha_{\mathbb{P}} - \alpha_{\mathbb{R}}))$ is the price one has to pay for a valence quark (and its corresponding flavor) to be exchanged between the two initial mesons. An additional price $\exp(-Y(1 - \alpha_{\mathbb{R}}))$ has to be paid if one exchanges a valence quark both in the initial and in the final state, which is what occurs in the $2 \rightarrow 2$ exclusive cross section.

In the following we shall assume $|C_{RL}(0,0)| \ll |p(1,0)| \sim 1$ which leads directly to $|\alpha_{\mathbb{P}} - 1| \ll 1$. Phenomenologically, the Pomeron intercept is $(\alpha_{\mathbb{P}} - 1) = 0.08 \pm 0.01$ [14]. Justifications for a small value of the $R - L$ correlator can be given using both dynamical and diagrammatic arguments. The short-range correlators within a single species are due, to a large extent, to the fact that the final stable particles very often result from the decay of resonances. However, the most prominent $q\bar{q}$ resonances can only occur in planar channels involving sets of “adjacent” (w.r.t. the planar diagram ordering) final particles. No such resonances can appear in “mixed” channels, i.e. those containing final particles of both species. The (not completely unrelated) diagrammatic argument consists of the observation that final particles belonging to different species are far away in high order Feynman diagrams that dominate the large distance QCD dynamics. Thus, intuitively, their momentum distributions should be weakly correlated. We can rephrase this last observation by saying that the two excited strings resulting from having separated two $q\bar{q}$ pairs in momentum and position phase space should fragment independently. These considerations will also apply to the processes discussed in the forthcoming sections.

4 Feynman-Wilson gas with baryons

In this Section we discuss processes with either one or two (anti)baryons in the initial state. For pedagogical reasons it is easier to describe first the process $B\bar{B} \rightarrow mesons$. We will then see that quantities related to that process also appear in other contexts, including baryon transport in meson-baryon scattering, baryon transport in BB and $B\bar{B}$ scattering, and $B\bar{B}$ pair creation in generic processes.

4.1 FWG for baryon-antibaryon annihilation

We will discuss the physically relevant case with $N_c = 3$ and for now, as explained in the introduction, limit our considerations to diagrams with the simplest topology consistent with the picture of baryons as a Mercedes star with quarks at the ends and the three ($N_c = 3$) Wilson lines joining in a point (junction) to make a gauge invariant operator. This structure, developed in ref. [1] as a natural extension of the notion of topological expansion in the presence of baryons, was corroborated by the results of ref. [7].

In that approximation the FWG for $B\bar{B} \rightarrow mesons$ consists of a gas with three distinct species (associated with each “page” of the baryon “book” topology), so that, in analogy

⁵The prediction $\alpha_{\mathbb{P}} = 1$ was also derived by H. Lee [22] under the stronger assumption of no correlations even within each species.

with (3.1), we define:

$$\Sigma_{ann}(z_1, z_2, z_3) = \frac{1}{\sigma_t^{ann}} \sum_{n_1+n_2+n_3 \geq 2} z_1^{n_1} z_2^{n_2} z_3^{n_3} \sigma^{ann}(n_1, n_2, n_3) \Rightarrow \Sigma_{ann}(1, 1, 1) = 1 \quad (4.1)$$

where σ_t^{ann} is the total annihilation cross section. With a straightforward generalization of (3.2) we rewrite Equation (4.1) in the form:

$$\begin{aligned} \Sigma_{ann}(z_1, z_2, z_3) &\equiv e^{Y p(z_1, z_2, z_3)} = \\ &= \exp \left(Y \sum_{m_1+m_2+m_3 \geq 1} c(m_1, m_2, m_3) \frac{(z_1-1)^{m_1} (z_2-1)^{m_2} (z_3-1)^{m_3}}{m_1! m_2! m_3!} \right) \end{aligned} \quad (4.2)$$

and then split $p(z_1, z_2, z_3)$ in terms of correlations with one species, two species and all the three species:

$$\begin{aligned} p(z_1, z_2, z_3) &= p_1(z_1) + p_2(z_2) + p_3(z_3) + C_{12}(z_1, z_2) + C_{13}(z_1, z_3) + C_{23}(z_2, z_3) + C_{123}(z_1, z_2, z_3), \\ p_i(z_i) &= \sum_{m_i \geq 1} c(m_i, 0, 0) \frac{(z_i-1)^{m_i}}{m_i!}, \quad i = 1, 2, 3 \\ C_{12}(z_1, z_2) &= \sum_{m_1, m_2 \geq 1} c(m_1, m_2, 0) \frac{(z_1-1)^{m_1} (z_2-1)^{m_2}}{m_1! m_2!}; \quad + \text{cyclic} \\ C_{123}(z_1, z_2, z_3) &= \sum_{m_1, m_2, m_3 \geq 1} c(m_1, m_2, m_3) \frac{(z_1-1)^{m_1} (z_2-1)^{m_2} (z_3-1)^{m_3}}{m_1! m_2! m_3!} \end{aligned} \quad (4.3)$$

Three equations come out of (4.3) after using $p_i(1) = C_{ij}(1, z_j) = C_{123}(1, z_j, z_k) = 0$, namely

$$\begin{aligned} p(1, 1, 0) - p_{ann}(0) &= 0; \\ 0 &= p(1, 1, 0) + \text{cycl} - p(1, 0, 0) - \text{cycl} + p(0, 0, 0) - C_{123}(0, 0, 0); \\ 0 &= p(1, 0, 0) + \text{cycl} - 2p(0, 0, 0) + \sum_{ij} C_{ij}(0, 0) + 2C_{123}(0, 0, 0) \end{aligned} \quad (4.4)$$

where we have defined $p_i(0) = p_{ann}(0)$. Equations (4.4) then lead to the following relations among the different intercepts relevant to $B\bar{B}$ annihilation (see Fig. (4) and Table 1):

$$\begin{aligned} \alpha_{\mathbb{J}_0} - \alpha_{\mathbb{J}_2} &= -p_{ann}(0); \\ \alpha_{\mathbb{J}_0} - (2\alpha_{\mathbb{B}} - 1) &= 3(\alpha_{\mathbb{J}_2} - \alpha_{\mathbb{J}_4}) - C_3(0, 0, 0); \\ (\alpha_{\mathbb{J}_0} - \alpha_{\mathbb{J}_4}) &= 2(\alpha_{\mathbb{J}_0} - \alpha_{\mathbb{J}_2}) - C_2(0, 0) \end{aligned} \quad (4.5)$$

These relations, illustrated in Fig. (5), show how the equal splitting of the intercepts gets broken by the two and three-species correlations. However, without further input, they simply give the three intercepts $\alpha_{\mathbb{J}_0}, \alpha_{\mathbb{J}_2}, \alpha_{\mathbb{J}_4}$ in terms of the (known) value $\alpha_{\mathbb{B}} \sim 0$ and the three unknown parameters $p_{ann}(0), C_{ij}(0, 0)$ and $C_{123}(0, 0, 0)$. In the following and in the figures we will simplify notations and write $C_{ij}(0, 0) \equiv C_2, C_3(0, 0, 0) \equiv C_3$.

An interesting open question is whether one can relate the jumps in pressure at the cylinder or planar level to those encountered in $B\bar{B}$ annihilation. In the case in which

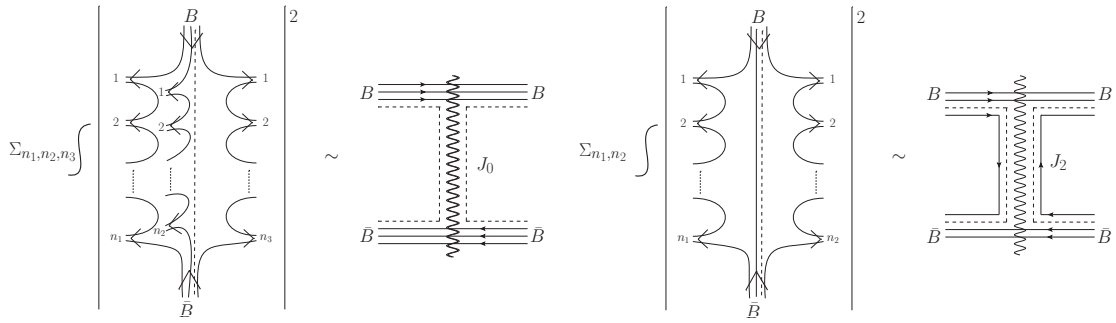


Figure 4. First two pictures from the left: total $B\bar{B}$ annihilation cross section and the Regge-pole J_0 controlling its high-energy limit. Last two pictures: $B\bar{B}$ annihilation cross section with a s -channel $q\bar{q}$ annihilation and the Regge-pole J_2 controlling its high-energy limit.

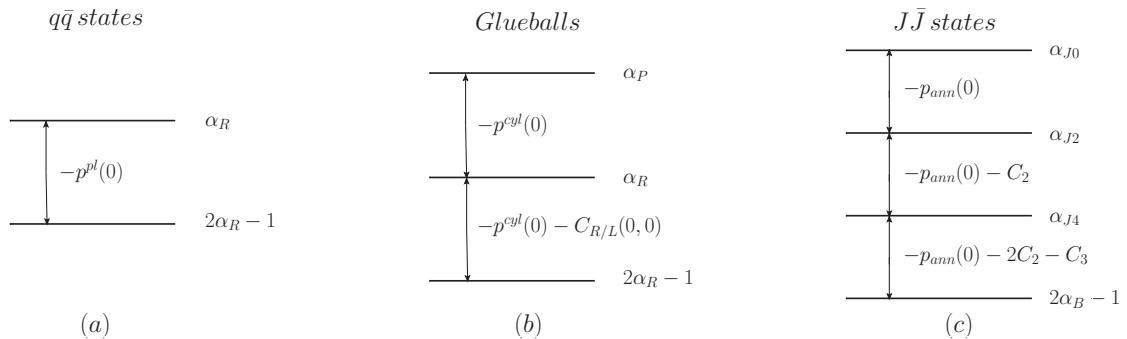


Figure 5. Intercepts of the Regge poles controlling the different cross sections discussed in Sections 2 and 3. The same intercepts will appear in the rapidity dependence of flavor and baryon-number transport discussed in Section 6. In this figure for uniformity we have introduced the following notations. We have denoted by $p^{pl}(0)$ the “planar” pressure $p(0)$ defined in Equation (2.2), by $p^{cyl}(0)$ the “cylinder” pressure $p_L(0) = p_R(0)$ defined in Equation (3.3) and by $p_{ann}(0)$ the pressure $p_i(0)$ defined in Equation (4.3).

inter-species correlations are neglected it is reasonable to assume that they are all the same and this leads to the predictions made in [1]. However, in the presence of inter-species correlations there is some ambiguity on how to connect the pressures in different processes.

One possibility is to identify $p_{ann}(0)$ in (4.4) with the individual pressure at the cylinder level, $p^{cyl}(0) = \alpha_{\mathbb{R}} - \alpha_{\mathbb{P}}$, defined in Fig. 5, and C_2 of (4.3) with $C_{RL}(0,0)$ in (3.3) i.e. with $(\alpha_{\mathbb{P}} - 1)$. In this case we predict:

$$\begin{aligned}
 \alpha_{\mathbb{J}_4} &= (2\alpha_{\mathbb{B}} - 1) + (1 - \alpha_{\mathbb{P}}) + (1 - \alpha_{\mathbb{R}}) - C_3 \sim -0.5 - C_{RL} - C_3 \\
 \alpha_{\mathbb{J}_2} &= (2\alpha_{\mathbb{B}} - 1) + (1 - \alpha_{\mathbb{P}}) + 2(1 - \alpha_{\mathbb{R}}) - C_3 \sim 0 - C_{RL} - C_3 \\
 \alpha_{\mathbb{J}_0} &= (2\alpha_{\mathbb{B}} - 1) + 3(1 - \alpha_{\mathbb{R}}) - C_3 \sim 0.5 - C_3
 \end{aligned} \tag{4.6}$$

Interestingly, with this identification the value of $\alpha_{\mathbb{J}_0}$ turns out to be the same as the original one [1] up to the three-species correlation C_3 . It is reasonable to expect that such

high-order correlation is even smaller than $C_{RL} \sim (\alpha_{\mathbb{P}} - 1)$.

Another possibility is to identify $p_{ann}(0)$ in (4.4) with the pressure at the planar level, $p(0)$ in (2.3) i.e. with $\alpha_{\mathbb{R}} - 1 \sim -0.5$ while still associating C_2 with $(\alpha_{\mathbb{P}} - 1)$. In this case we would predict instead of Eq.(4.6):

$$\begin{aligned}\alpha_{\mathbb{J}_4} &= (2\alpha_{\mathbb{B}} - 1) + 2(1 - \alpha_{\mathbb{P}}) + (1 - \alpha_{\mathbb{R}}) - C_3 \sim -0.5 - 2C_{RL} - C_3 \\ \alpha_{\mathbb{J}_2} &= (2\alpha_{\mathbb{B}} - 1) + 3(1 - \alpha_{\mathbb{P}}) + 2(1 - \alpha_{\mathbb{R}}) - C_3 \sim 0 - 3C_{RL} - C_3 \\ \alpha_{\mathbb{J}_0} &= (2\alpha_{\mathbb{B}} - 1) + 3(1 - \alpha_{\mathbb{P}}) + 3(1 - \alpha_{\mathbb{R}}) - C_3 \sim 0.5 - 3C_{RL} - C_3\end{aligned}\quad (4.7)$$

The data favors this option; if we take $C_{RL} = 0.08$, and $C_3 = 0$, we reproduce the data. Indeed, we get $\alpha_{\mathbb{J}_0} \simeq 0.26$ yielding the beam rapidity dependence $e^{(\alpha_{\mathbb{J}_0} + \alpha_{\mathbb{P}} - 2)Y/2} = e^{-0.66 Y/2}$ in Eq. (1.4), to be compared to the STAR experimental result $e^{-0.65 Y/2}$ [13].

Note that if the C_{RL} and C_3 correlations were negligible, the two predictions outlined above in Eq.(4.6) and Eq.(4.7) would agree and give back the original estimates of [1].

5 Regge trajectories and spectra of the junction-antijunction glueballs

Here we will try to relate the J_0 trajectory to the spectroscopy of potential junction-antijunction glueballs. We will assume the usual linear Regge trajectory

$$\alpha(M^2) = \alpha(0) + \alpha' M^2, \quad (5.1)$$

relating the spin and mass of hadrons on the trajectory. Thus, the intercept $\alpha(0)$ can be extracted if one knows the spin and mass of any particle on the trajectory, as well as the slope α' .

The QCD operator corresponding to the junction-antijunction J_0 glueball is given by a contraction of three Wilson lines [1] (see Eq. (1.1)):

$$G_{J\bar{J}}(x, y) = \epsilon^{ijk} \epsilon_{i'j'k'} [U(C_1(x, y))]_i^{i'} [U(C_2(x, y))]_j^{j'} [U(C_3(x, y))]_k^{k'}, \quad (5.2)$$

where the integrations are along three different paths, C_1, C_2 and C_3 . Note that this operator does *not* go into \pm itself under charge conjugation \mathcal{C} . Indeed it goes to a similar operator where junction and antijunction are exchanged and, at the same time, the directions of the three Wilson lines are reversed. On the other hand it is clear that the new state has the same mass spectrum as the original one because QCD respects \mathcal{C} -invariance.⁶ The above argument suggests that the J_0 Regge pole actually corresponds to two degenerate \mathcal{C} -related Regge poles of opposite signature, denoted by f_0^J and ω_0^J in Ref. [1]. Their degeneracy ensures that they combine to give a purely real amplitude in BB scattering corresponding to the absence of an annihilation channel there. Obviously this degeneracy will be lifted if the two \mathcal{C} -eigenstates mix with other states with the same \mathcal{C} , such as \mathbb{P} for f_0^J and ω for ω_0^J . However, this mixing should be suppressed by the JOZI rule (see [9] for a discussion of the JOZI rule).

Let us see how the \mathcal{C} parity of the J_0 states can be described in a perturbative language. We will start by performing the expansion of the operator (5.2) up to the 2-gluon order,

⁶Under \mathcal{C} the states J_2 and J_4 get transformed into their antiparticles.

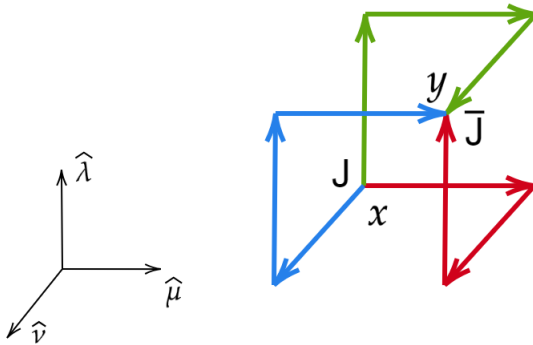


Figure 6. A possible lattice operator that can be used to search for the J_0 glueball. The color is antisymmetrized at each of the junctions. Directions on the lattice are introduced in accordance with Eq. (5.3).

$\mathcal{O}(g^2)$. With each Wilson line expanded to 0, 1 or 2 orders the following contributions are present in the expansion:

- $\mathcal{O}(g) \times \mathcal{O}(g) \times \mathcal{O}(1) : G_{gg1} = g^2 \text{tr} \left(\int_{C_1} A \int_{C_2} A + 2 \text{ permutations} \right)$
- $\mathcal{O}(g^2) \times \mathcal{O}(1) \times \mathcal{O}(1) : G_{g^211} = -g^2 \text{tr} \left(P \left(\int_{C_1} A \right)^2 + 2 \text{ permutations} \right)$.

Here we used the shorthand notation:

$$\int_{C_1} A \equiv \int_{C_1(x,y)} dz^\mu A_\mu(z); \quad P \left(\int_{C_1} A \right)^2 \equiv \int_{C_1(x,y)} dz^\mu A_\mu(z) \int_{C_1(x,z)} dz'^\nu A_\nu(z').$$

Under the \mathcal{C} -conjugation the gluon field (which is a $SU(3)$ matrix) transforms like $A \rightarrow -A^T$ as can be seen from its coupling to the quark fields in the QCD Lagrangian ⁷. Therefore, both terms in the 2-gluon expansion are \mathcal{C} -even.

Let us now discuss the properties of the corresponding Regge trajectories. The 2-gluon state in the S -wave (corresponding to the lowest-lying state on the Regge trajectory) is \mathcal{P} -even. Since we are interested in the leading J_0 Regge trajectory, we need to identify the S -wave two gluon state with the highest spin. This is a spin 2 state.

A glueball state with $J^{\mathcal{PC}} = 2^{++}$ was reported in a quenched lattice calculation [23]. Even though it has the right quantum numbers, we do not expect it to be a J_0 glueball since the operator used in the computation did not include the junction-antijunction color structure. We thus propose to perform a lattice calculation of the J_0 masses using, for

⁷Since \mathcal{C} -conjugation acts on the fermion field as $C\psi C = -i(\bar{\psi}\gamma^0\gamma^2)^T$, $C\bar{\psi}C = -i(\gamma^0\gamma^2\psi)^T$, the transformation $CA_{\mu j}^i C = -A_{\mu i}^j$ ensures that the quark-gluon interaction term in the QCD Lagrangian is invariant under \mathcal{C} :

$$C\bar{\psi}_i\gamma^\mu A_{\mu j}^i\psi^j C = A_{\mu i}^j(\gamma^0\gamma^2\psi^i)^T\gamma^\mu(\bar{\psi}_j\gamma^0\gamma^2)^T = -A_{\mu i}^j\bar{\psi}_j\gamma^0\gamma^2(\gamma^\mu)^T\gamma^0\gamma^2\psi^i = A_{\mu i}^j\bar{\psi}_j\gamma^\mu\psi^i$$

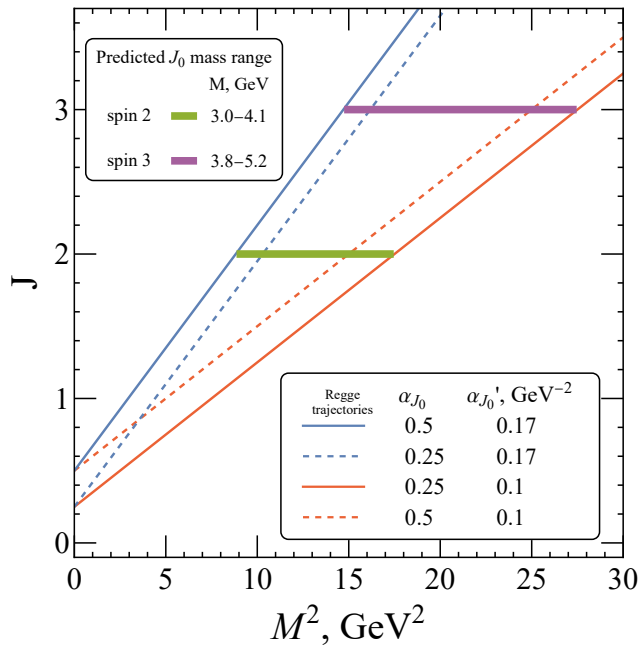


Figure 7. Leading J_0 Regge trajectories corresponding to the various values of the intercept. The predicted mass range of spin-two and spin-three glueballs is highlighted.

instance, the operator (5.2) with the three paths as depicted in Fig. (6):

$$O_{J_0} = \epsilon_{i_1 j_1 k_1} U_{i_2}^{i_1}(x, \hat{\mu}) U_{i_3}^{i_2}(x + \hat{\mu}, \hat{\nu}) U_{i_4}^{i_3}(x + \hat{\mu} + \hat{\nu}, \hat{\lambda}) U_{j_2}^{j_1}(x, \hat{\nu}) U_{j_3}^{j_2}(x + \hat{\nu}, \hat{\lambda}) U_{j_4}^{j_3}(x + \hat{\nu} + \hat{\lambda}, \hat{\mu}) U_{k_2}^{k_1}(x, \hat{\lambda}) U_{k_3}^{k_2}(x + \hat{\lambda}, \hat{\mu}) U_{k_4}^{k_3}(x + \hat{\lambda} + \hat{\mu}, \hat{\nu}) \epsilon^{i_4 j_4 k_4}, \quad (5.3)$$

where $U_j^i(x, \hat{\mu})$ denotes a gauge link operator originating at point x in the direction $\hat{\mu}$, see Fig. 6 for notations.

To predict the mass of the $J^{PC} = 2^{++}$ J_0 glueballs, we need to know the slope of the J_0 Regge trajectory. One can relate this slope to the slope of the Pomeron trajectory. Since the Pomeron exchange corresponds to a closed string, we can estimate the J_0 trajectory slope to be

$$\alpha'_{J_0} \simeq \frac{2}{3} \alpha'_{\mathbb{P}} \simeq 0.10 - 0.17 \text{ GeV}^{-2}, \quad (5.4)$$

where the numerical value is obtained by using the Pomeron slope in the range $\alpha'_{\mathbb{P}} \simeq 0.15 - 0.25 \text{ GeV}^{-2}$ corresponding to various estimates [14, 24]. Using the intercept of the leading J_0 Regge trajectory $\alpha_{J_0} \simeq 0.25 - 0.5$, we obtain the prediction for the $J^{PC} = 2^{++}$ J_0 glueball mass in the range of $M_{J_0} = 3.0 - 4.1 \text{ GeV}$. These values of the mass are highlighted in Fig. (7) together with the Regge trajectories constraining the mass range as discussed above.

It is also instructive to repeat this analysis in the case of the 3-gluon terms in the expansion of (5.2). One obtains the following $\mathcal{O}(g^3)$ terms:

- $\mathcal{O}(g) \times \mathcal{O}(g) \times \mathcal{O}(g) : G_{ggg} = -i g^3 \text{tr} \left(\int_{C_1} A \int_{C_2} A \int_{C_3} A + \int_{C_1} A \int_{C_3} A \int_{C_2} A \right),$

- $\mathcal{O}(g^2) \times \mathcal{O}(g) \times \mathcal{O}(1) : G_{g^2g1} = \frac{ig^3}{2} \text{tr} \left(P(\int_{C_1} A)^2 \int_{C_2} A + 5 \text{ permutations} \right),$
- $\mathcal{O}(g^3) \times \mathcal{O}(1) \times \mathcal{O}(1) : G_{g^311} = -\frac{ig^3}{3} \text{tr} \left(P(\int_{C_1} A)^3 + P(\int_{C_2} A)^3 + P(\int_{C_3} A)^3 \right),$

where the following additional notation was introduced:

$$P \left(\int_{C_1} A \right)^3 \equiv \int_{C_1(x,y)} dz^\mu A_\mu(z) \int_{C_1(x,z)} dz'^\nu A_\nu(z') \int_{C_1(x,z')} dz''^\lambda A_\lambda(z'').$$

Along the lines of the previous \mathcal{C} -parity discussion, the G_{ggg} term is \mathcal{C} -odd. Indeed, it is easy to see that the operator G_{ggg} includes only terms containing the symmetric structure constants, $d_{abc} \propto \text{tr}(\lambda^a \lambda^b \lambda^c + \lambda^a \lambda^c \lambda^b)$. Such symmetric 3-gluon combinations are indeed \mathcal{C} -odd, see e.g. [25]. On the other hand, G_{g^2g1} and G_{g^311} are a mixture of \mathcal{C} -even and \mathcal{C} -odd operators because under \mathcal{C} -conjugation $P(\int_{C_1} A)^n \rightarrow (-1)^n \bar{P}(\int_{C_1} A)^n$, where \bar{P} denotes inverse path-ordering.

The 3-gluon state in the S -wave is \mathcal{P} -odd, therefore the highest-spin 3-gluon component of the J_0 can be $J^{\mathcal{P}\mathcal{C}} = 3^{--}$ and $J^{\mathcal{P}\mathcal{C}} = 3^{-+}$. Estimate for the masses of these glueballs similar to those provided by Eq. (5.4) yield values that fall in the range of 3.8 – 5.2 GeV as displayed in Fig. 7.

The large uncertainty in the range of J_0 glueball masses thus predicted is mainly due to the uncertainty of the Pomeron trajectory slope (5.4) that we use to estimate the slope of the J_0 trajectory. In Section 7 we suggest a way to extract the slope of the J_0 trajectory directly from doubly-diffractive baryon-antibaryon pair creation in pp or ep collisions. Such a measurement would allow to further narrow down the range of the glueball masses that we expect to be found in the lattice simulations.

6 Transport of flavor and baryon number

In this section we extend the arguments of the previous sections to the study of inclusive spectra as a function of rapidity (i.e. after integration over the transverse momenta). The main point we wish to make is that, in the topological expansion approach, flavor and baryon number transport over large rapidity intervals are very weakly correlated. Furthermore, the exponents that control the exponential decay of the various inclusive cross sections as a function of rapidity intervals are not independent and the relations between them can be predicted theoretically and checked against the data.

The tools that we will employ in this part of the paper are those discussed in the Sections 2, 3 and 4 up to two important extensions:

- We shall need the more detailed description of the inclusive cross sections. This could in principle include information about the transverse momenta of the detected final particles but for our purposes it will be sufficient to discuss distributions in rapidity y i.e. after integration over the (assumed strongly cut-off) transverse momenta, see Appendix A for details. We will therefore deal with single particle distribution of the

type:

$$\rho(y_f) = \frac{1}{\sigma_t^{cyl}} \frac{d\sigma^{cyl}(1+2 \rightarrow y_f + X)}{dy_f} \quad (6.1)$$

and with their generalization to the multiparticle distributions defined in Appendix A.

- We will also use Mueller and Kancheli's extension [11, 12] of the optical theorem and Regge pole analysis to evaluate the inclusive cross sections.

We stress again that, as in the previous Sections, all this will be done in the context of the TE of QCD [5].

6.1 Quark/ flavor transport in meson-meson scattering

Let us first consider, at the bare-Pomeron level, the rapidity dependence of quark transport from the fragmentation regions $y \sim \pm Y/2$ to some y such that $|\pm Y/2 - y| \gg 1$. If the valence quark to be transported is the one initially at $y \sim Y/2$, one can analyze the single particle distribution (6.1) using the Mueller-Kancheli generalized optical theorem [11, 12].

The Mueller-Kancheli diagram describing this inclusive cross section is dominated by the leading $q\bar{q}$ Regge trajectory from $y = Y/2$ down to $y = y_f$ and by the bare-Pomeron pole from $y = y_f$ to $y = -Y/2$ (see right panel in Fig. (8)). In drawing the Mueller-Kancheli diagram we use the convention of showing in each $t = 0$ channel, the quark and or junction lines that flow through the corresponding rapidity gap.

For instance, in Fig. (8) we are considering the regime: $|\pm Y/2 - y_f| \gg 1$. If the valence quark to be transported is initially at $y \sim Y/2$ then the leading trajectory in the interval $[Y/2 - y_f]$ contains a $q\bar{q}$ pair whereas the trajectory determining the leading behaviour at large $[y_f + Y/2]$ is the vacuum (Pomeron) trajectory. As a result one predicts the single particle distribution (6.1) to behave as

$$\begin{aligned} \rho(y_f) &\sim \exp(-Y\alpha_{\mathbb{P}}) \exp(\Delta y \alpha_{\mathbb{R}}) \exp((Y - \Delta y)\alpha_{\mathbb{P}}) \\ &= \exp(-\Delta y(\alpha_{\mathbb{P}} - \alpha_{\mathbb{R}})) ; \quad \Delta y \equiv (Y/2 - y_f) \end{aligned} \quad (6.2)$$

where the first exponential comes from the normalization factor σ_t^{cyl} in the definition (6.1).

In analogy with what we discussed at the end of Section 3.1 we see that the price to be paid for transporting a quark from $y = Y/2$ to $y = y_f$ is given by (recall the second line of eq. (3.6))

$$\exp(-|Y/2 - y_f|(\alpha_{\mathbb{P}} - \alpha_{\mathbb{R}})) = \exp(-|Y/2 - y_f|(1 + C_{RL}(0,0) - \alpha_{\mathbb{R}})) \quad (6.3)$$

In the limiting case in which $y_f = -Y/2$ we recover the penalty $\exp(-Y(\alpha_{\mathbb{P}} - \alpha_{\mathbb{R}}))$ discussed in Section 3.1 for annihilating a quark between the two initial mesons. Furthermore, one expects quark transport to be accompanied by a reduced multiplicity (by about a factor 2) in the rapidity interval $[Y/2 - y_f]$ compared to the complementary interval $[y_f - (-Y/2)]$, because in one case we cut a Reggeon/plane and in the other a Pomeron/cylinder.

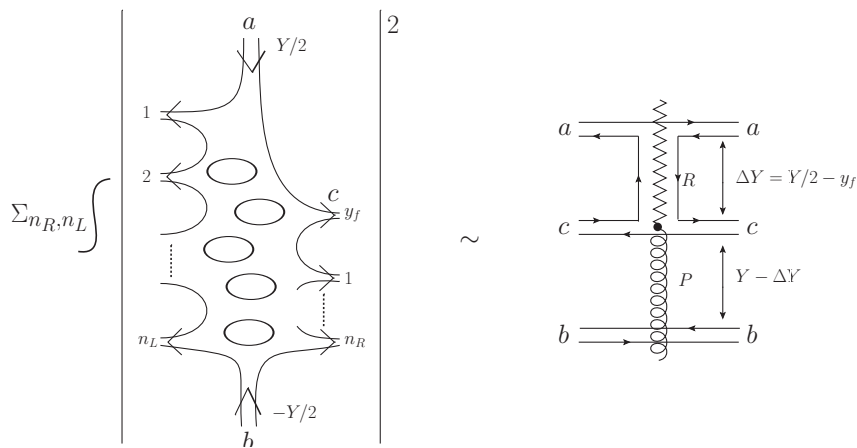


Figure 8. Flavor transport in rapidity in MM scattering and its corresponding Mueller-Kancheli diagram leading to (6.2).

It is interesting theoretically to discuss the total transfer in rapidity of a given conserved flavor $Q^{(i)}$ ($i = u, d, s, \dots$) carried by the initial mesons. In order to compute such a quantity we would have to sum the contribution to $Q^{(i)}$ coming from each individual meson's inclusive cross section. This is quite a hard task that we leave to further investigations. However, we can use some sort of completeness argument (often used in jet-physics or heavy quark fragmentation) to connect directly the rapidity distribution of the valence quark in the final state as tracing the total transfer of the particular charge it carries. The idea is that somehow that charge will have to be deposited in *some* meson sitting at the quark's rapidity.

With this proviso, we can readily give the (Y, y_f) dependence of the charge distribution in the final state in a form similar to the one given in Eq. (1.4) for the baryon-number distribution:

$$\frac{dQ^{(i)}}{dy_f} \propto e^{(\alpha_i + \alpha_{\mathbb{P}} - 2)Y/2} [g_{ia} e^{(\alpha_{\mathbb{P}} - \alpha_i)y_f} + g_{ib} e^{(\alpha_i - \alpha_{\mathbb{P}})y_f}], \quad (6.4)$$

where α_i stands for (the intercept of) the leading $q_i \bar{q}_i$ trajectory ($\alpha_i = \alpha_{\rho}$ for $i = u, d$; $\alpha_i = \alpha_{\phi}$ for $i = s, \dots$) and g_{ia}, g_{ib} are the couplings of that trajectory to the two initial particles. Note that, unlike the case of the inclusive single particle cross section (6.2), we are not normalizing the distribution to the total cylinder cross section.

One can consider linear combinations of the above expressions in order to describe, for instance, the transport of electric-charge $Q \sim \frac{2}{3}Q^{(u)} - \frac{1}{3}Q^{(d)} - \frac{1}{3}Q^{(s)}$ that can be directly measured in experiment. On the other hand it is easy to check that no net charge transport occurs for the combination $B \equiv \frac{1}{3} \sum_i Q^{(i)}$ corresponding to baryon number. For this to happen one needs at least one baryon in the initial state as discussed in the following sub-sections.

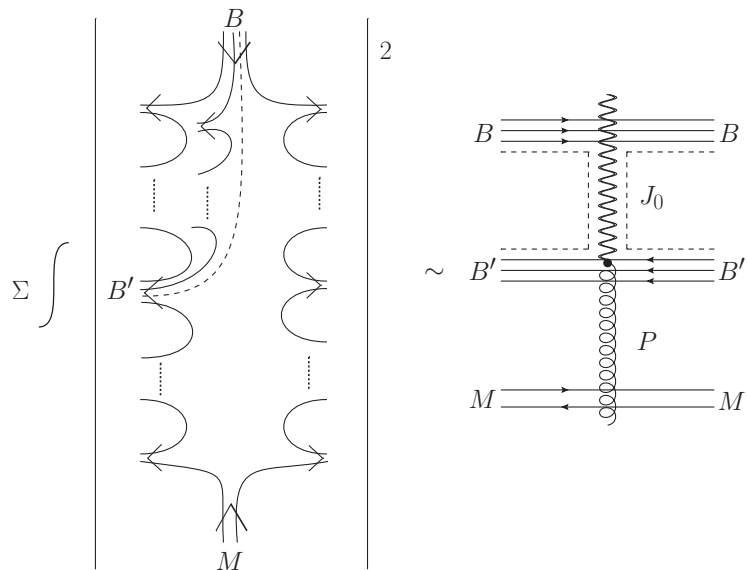


Figure 9. Baryon-number (without valence quarks) transport in MB scattering and its corresponding Mueller-Kancheli diagram leading to equation (6.5).

6.2 Baryon and flavor transport in meson-baryon scattering

The case of meson-baryon scattering is very similar to the one of meson-meson scattering as far as flavor transport is concerned. In particular, Eqs. ((6.2)), (6.4) are still valid. The process is analogous to the one shown in Fig. (8) with particle a being now a baryon.

However, a new feature now appears, namely baryon-number transport. In other words, if we fix the initial baryon’s rapidity to be $+Y/2$, we can ask what is the inclusive rapidity distribution of a final baryon sitting at some y_f . Proceeding in analogy with our treatment of conserved-charge transfer in meson-meson scattering we may first consider the inclusive cross section for a given final baryon and get, in analogy with ((6.2)),

$$\rho_B(y_f) \sim \exp[-|Y/2 - y_f|(\alpha_{\mathbb{P}} - \alpha_{\mathbb{J}_0})] \sim \exp(-0.82 |Y/2 - y_f|), \quad (6.5)$$

where we have used the value of $\alpha_{\mathbb{J}_0}$ from Eq.(4.7). The corresponding Mueller-Kancheli diagram is shown in Fig. (9).

As in the case of flavor transport in meson-meson scattering we can consider the “super-inclusive” baryon-number distribution, i.e. summed over the individual single baryons. The resulting distribution (not normalized to the total cross section) will have the following rapidity dependence:

$$\frac{dN}{dy_f} \propto e^{(\alpha_{\mathbb{J}_0} + \alpha_{\mathbb{P}} - 2)Y/2} e^{(\alpha_{\mathbb{P}} - \alpha_{\mathbb{J}_0})y_f}, \quad (6.6)$$

with much similarity with Eq. (1.4).

Quite exceptionally, one or more of the initial quarks may end up in the final baryon. The corresponding rapidity distribution would be dominated by the J_2 and J_4 trajectories

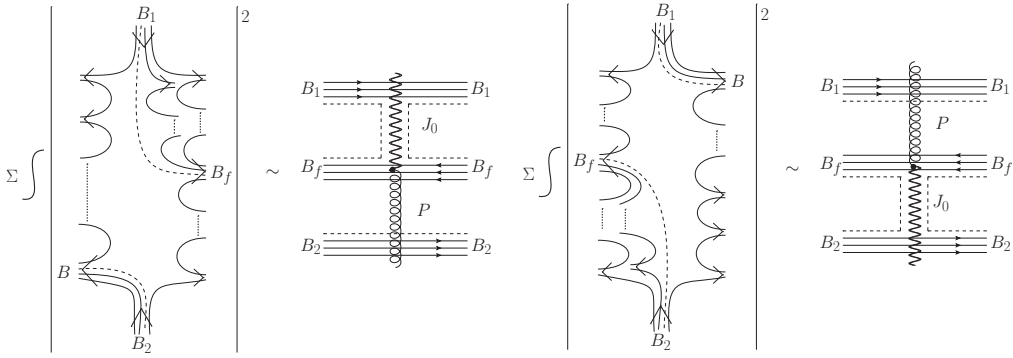


Figure 10. Left panel: baryon-number (without flavor) transport in BB scattering via the junction of B_1 and its corresponding Mueller-Kancheli diagram. Right panel: the same but with baryon-number transport via the junction of B_2 . The two contributions are added up in (6.9).

according to

$$\begin{aligned}\rho_B(y_f) &\sim \exp[-|Y/2 - y_f|(\alpha_{\mathbb{P}} - \alpha_{\mathbb{J}_2})], \\ \rho_B(y_f) &\sim \exp[-|Y/2 - y_f|(\alpha_{\mathbb{P}} - \alpha_{\mathbb{J}_4})],\end{aligned}\tag{6.7}$$

for one and two transported quarks, respectively. We postpone the discussion of joint baryon-number-charge transfer to the case of baryon-baryon scattering presented in the following subsection.

6.3 Baryon and flavor transport in baryon-(anti)baryon scattering

We now move to baryon-(anti)baryon scattering which, together with its extension to heavy-ion collisions, is of course the most interesting case. The difference with respect to the MB case discussed in the previous subsection is that we now have either two junctions or a junction-antijunction pair in the initial state. We have already discussed, in Section (4.1), the case of $B\bar{B}$ (i.e. junction-antijunction) annihilation. Here we will consider instead the case in which the baryon-number connected with an initial junction (or antijunction) is transported towards small rapidities. We will do so while still neglecting baryon-antibaryon pair creation, a topic discussed at the end of this Section.

As discussed in the previous subsection, the leading contribution will come from J_0 exchange:

$$\rho_B(y_f) \sim \exp[-|Y/2 - y_f|(\alpha_{\mathbb{P}} - \alpha_{\mathbb{J}_0})] \sim \exp(-0.82|Y/2 - y_f|).\tag{6.8}$$

Actually, the only difference with respect to MB scattering is that now the transported baryon number can come from either one of the two initial baryons. Therefore, a term with $Y/2 \rightarrow -Y/2$ has to be added to (6.8). The single-baryon inclusive cross section is thus

$$\rho_B(y_f) \sim e^{-(\frac{Y}{2} - y_f)(\alpha_{\mathbb{P}} - \alpha_{\mathbb{J}_0})} + e^{-(\frac{Y}{2} + y_f)(\alpha_{\mathbb{P}} - \alpha_{\mathbb{J}_0})} = 2e^{-\frac{Y}{2}(\alpha_{\mathbb{P}} - \alpha_{\mathbb{J}_0})} \cosh[y(\alpha_{\mathbb{P}} - \alpha_{\mathbb{J}_0})]\tag{6.9}$$

This situation is illustrated in Fig. (10). Once more it makes more sense, experimentally, to trace baryon-number transport “super-inclusively” i.e. without reference to the specific

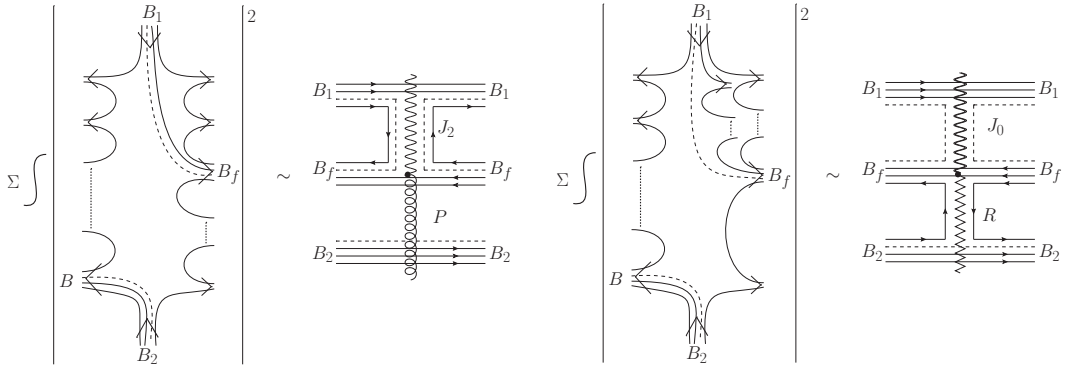


Figure 11. Left panel: baryon-number plus one-quark transport from B_1 and its corresponding Mueller-Kancheli diagram leading to (6.10). Right panel: baryon-number transport from B_1 together with a one-quark-transport from B_2 and its corresponding Mueller-Kancheli diagram leading to eq. (6.11).

baryon detected in the final state. Arguing as in the cases of meson-meson and meson-baryon scattering, Eq. (6.9) leads precisely to Eq. (1.4).

One may also consider the (unlikely) case in which the observed final baryon transports to rapidity y_f both the junction and one quark of B_1 . This will give

$$\rho_B(y_f) \sim e^{-(\frac{Y}{2}-y_f)(\alpha_P-\alpha_{J_2})} \quad (6.10)$$

as illustrated in Fig. (11) (left panel), while the case in which the observed baryon transports the junction of B_1 and one valence quark of B_2 , yields

$$\rho_B(y_f) \sim e^{-(\frac{Y}{2}-y_f)(\alpha_P-\alpha_{J_0})} e^{-(\frac{Y}{2}+y_f)(\alpha_P-\alpha_R)} \quad (6.11)$$

This case is illustrated in Fig. (11) (right panel). These processes are suppressed with respect to J_0 exchange (no valence quark transport), described by Eq.(6.9).

6.4 Combined charge–baryon-number rapidity distribution

Let us finally come to the very interesting topic of the combined baryon-number/ charge transport in baryon-baryon collisions, a quantity which is expected to neatly differentiate between the junction and the valence-quark pictures for the tracing of baryon number. To this purpose we have to consider a two-particle inclusive cross section or, even better, a joint distribution of charge and baryon number. In the junction picture it is unlikely for one of the initial junctions and one of the initial valence quarks to end up in the same baryon sitting at small y_f . Much more frequently, the valence quark will end up in a meson. Consider then the combined baryon-number–charge distribution:

$$\frac{d^2\sigma_{(B,Q)}}{dy_B dy_Q} \equiv F_{(B,Q)}(Y, y_B, y_Q), \quad (6.12)$$

as an extension of the separate flavor and baryon-number distributions discussed so far.

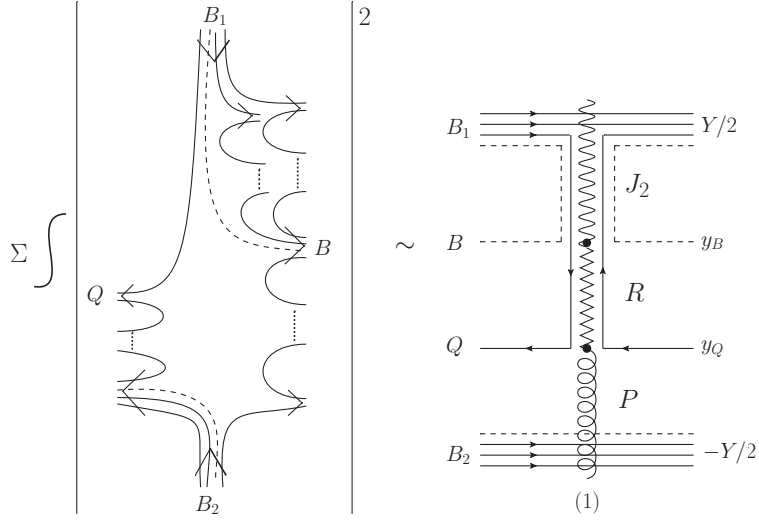


Figure 12. Diagrams contributing to charge–baryon-number separation and the corresponding Mueller-Kancheli diagram leading to the first of Eqs. (6.13). The single quark and junction lines stand for a sum over all the hadrons containing those lines.

With arguments basically identical to those used for each separate distributions it is straightforward to discuss the dependence of $F_{(B,Q)}$ both on the total rapidity Y and on the rapidity differences $|(\pm \frac{Y}{2} - y_B)|$, $|(\pm \frac{Y}{2} - y_Q)|$, $|y_B - y_Q|$ all taken to be sufficiently large. The number of distinct cases is a bit larger than in the single-distribution case, but still quite manageable. Up to a trivial exchange of the two incoming baryons, we can identify four distinct cases whose Mueller-Kancheli diagrams are given in Figs. (12) and (13). The corresponding distributions are given by:

$$\begin{aligned}
F_{(B,Q)}^{(1)} &\propto e^{(\alpha_{\mathbb{P}} + \alpha_{\mathbb{J}_2} - 2)\frac{Y}{2}} e^{(\alpha_R - \alpha_{\mathbb{J}_2})y_B} e^{(\alpha_{\mathbb{P}} - \alpha_R)y_Q} , \\
F_{(B,Q)}^{(2)} &\propto e^{(\alpha_{\mathbb{P}} + \alpha_{\mathbb{J}_2} - 2)\frac{Y}{2}} e^{(\alpha_{\mathbb{J}_0} - \alpha_{\mathbb{J}_2})y_Q} e^{(\alpha_{\mathbb{P}} - \alpha_{\mathbb{J}_0})y_B} , \\
F_{(B,Q)}^{(3)} &\propto e^{(\alpha_R + \alpha_{\mathbb{J}_0} - 2)\frac{Y}{2}} e^{(\alpha_{\mathbb{P}} - \alpha_R)y_Q} e^{(\alpha_{\mathbb{J}_0} - \alpha_{\mathbb{P}})y_B} , \\
F_{(B,Q)}^{(4)} &\propto e^{(\alpha_R + \alpha_{\mathbb{J}_0} - 2)\frac{Y}{2}} e^{(\alpha_{\mathbb{J}_0} - \alpha_{\mathbb{J}_2})y_Q} e^{(\alpha_{\mathbb{J}_2} - \alpha_R)y_B} .
\end{aligned} \tag{6.13}$$

As one can see from Figs. (12) and (13), the terms $F_{(B,Q)}^{(1)}$ and $F_{(B,Q)}^{(4)}$ contribute in the case of the rapidity ordering $-Y/2 < y_Q < y_B < Y/2$ while $F_{(B,Q)}^{(2)}$ and $F_{(B,Q)}^{(3)}$ correspond to the ordering $-Y/2 < y_B < y_Q < Y/2$. Of course, for a given y_B, y_Q all relevant contributions (including those related by some trivial symmetry to the ones of Figs.(12) and (13)) have to be included. Note that both J_0 and J_2 play an important role in the above formulae. Therefore, if it is possible to measure those double rapidity distributions with sufficient accuracy, one can extract not only the leading intercept $\alpha_{\mathbb{J}_0}$, but also $\alpha_{\mathbb{J}_2}$ and thus check the consistency of the framework.

Eq.(6.13) can be normalized by the total cross section $\sigma_t^{cyl} \sim e^{(\alpha_{\mathbb{P}} - 1)Y}$ to yield the

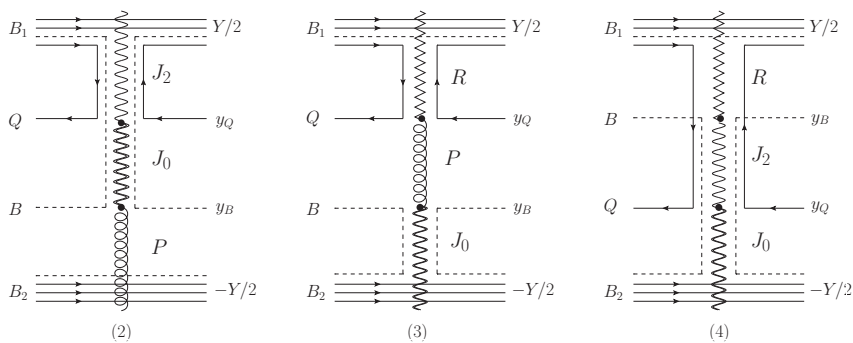


Figure 13. The Mueller-Kancheli diagrams leading, in the order, to the last three Eqs.(6.13). The single quark and junction lines stand for a sum over all the hadrons containing those lines.

combined flavor-baryon probability distributions of a kind similar to Eq.(6.1):

$$\rho_{(B,Q)}^{(i)} \propto e^{(1-\alpha_{\mathbb{P}})Y} F_{(B,Q)}^{(i)}. \quad (6.14)$$

Finally, we can consider the baryon-flavor correlation function:

$$C_{(B,Q)}(Y, y_B, y_Q) \equiv \frac{\rho_{(B,Q)}(Y, y_B, y_Q)}{\rho_B(y_B) \rho_Q(y_Q)} - 1, \quad (6.15)$$

study its dependence upon the flavor-baryon separation $\Delta y \equiv |y_B - y_Q|$, and contrast it with expectations in the valence-quark picture. We have checked that this correlation quickly vanishes as one increases Δy while keeping $|y_B + y_Q|$ small, but leave a detailed study of this important topic to future work.

6.5 Rapidity distribution of $B\bar{B}$ -pair creation

We may finally turn to a process we have so far ignored (since it should only provide small corrections for the cases we have previously considered) i.e. $B\bar{B}$ -pair production. This process can be thought of as a process $M^*M^* \rightarrow B\bar{B} + mesons$ in which the initial mesons are off-shell and spacelike. The process occurs through the creation of a junction-antijunction pair (presumably from a purely gluonic process). As long as the pair is not much separated in rapidity, this is a low-energy non-perturbative process we cannot say much about.

However, as one takes the pair to be well separated in rapidity, the two-particle (meaning $B\bar{B}$) distribution will fall off exponentially in $|\Delta y|$. The corresponding exponent is controlled again by the intercept of $J\bar{J}$ trajectories. If we do not veto meson production in the rapidity interval Δy , $\alpha_{\mathbb{J}_0}$ will provide the leading contribution for large $|\Delta y|$, giving

$$\rho_{B,\bar{B}}(\Delta y) \sim e^{-|\Delta y|(\alpha_{\mathbb{P}} - \alpha_{\mathbb{J}_0})}, \quad (6.16)$$

with subleading contributions coming from $\alpha_{\mathbb{J}_2}$, $\alpha_{\mathbb{J}_2}$. If, instead, meson production is completely vetoed, the 2-baryon cut intercept $(2\alpha_{\mathbb{B}} - 1)$ will replace $\alpha_{\mathbb{J}_0}$ in (6.16). The case corresponding to (6.16) is illustrated in Fig. (14). We stress again that no new input is

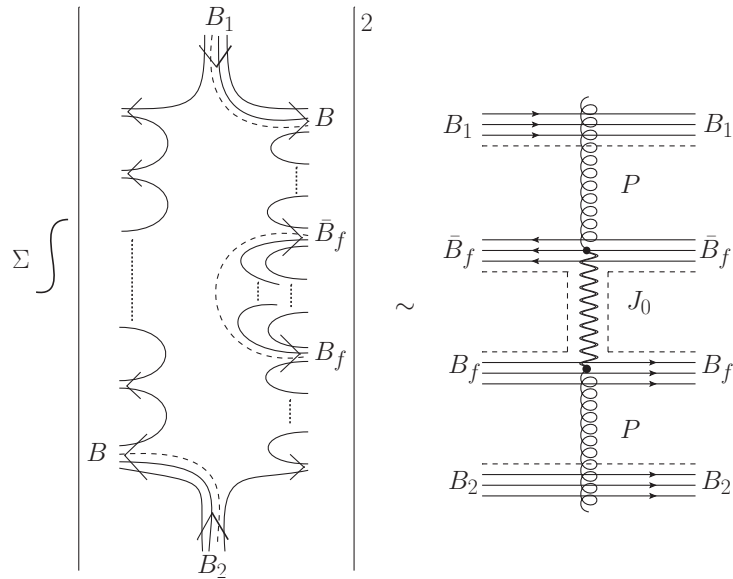


Figure 14. $B - \bar{B}$ pair creation and the corresponding Mueller-Kancheli diagram leading to (6.16).

needed in order to make these predictions. The universality and factorization of Regge poles ensures that the same trajectories control the asymptotic behavior of different measurable processes.

Let us now come back to the question of the role of $B\bar{B}$ -pair production in determining the physical Pomeron intercept discussed in Section 3 where $B\bar{B}$ -pair production was not included (although it is certainly in the data). It is quite obvious from Fig. (14) that from a Mueller-Kancheli point of view adding $B\bar{B}$ -pair production will amount to introducing a $\mathbb{P} - \mathbb{J}_0$ coupling and mixing which will eventually renormalize upwards the Pomeron intercept. This is allowed if we remember that J_0 has a positive \mathcal{C} , positive signature component which will mix with the Pomeron and thus contribute equally to BB and $B\bar{B}$ total cross sections. However, this mixing should be suppressed by the JOZI rule.

7 Predictions and experimental tests

Our suggestions and predictions for experiment and lattice calculations can be summarized as follows.

- The cleanest example of baryon-number – flavor separation is the stopping of Ω hyperons in pp or ep collisions. Observing it would represent a clear signature of the baryon-number – flavor separation phenomenon.
- At a more inclusive and quantitative level one should develop further the idea of computing and measuring the joined charge-baryon-number rapidity distribution as a function of their rapidity separation. This where the junction picture should drastically differ from the conventional one associating the flow of baryon number to that of the valence quarks.

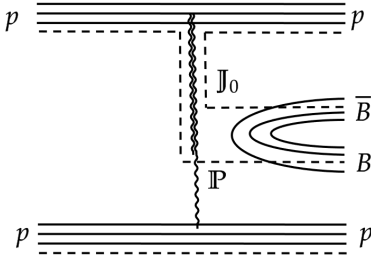


Figure 15. Double-diffractive production of $B\bar{B}$ pair that can be used to extract the slope of the J_0 trajectory.

- One needs to confirm the energy and rapidity dependence of single baryon stopping, and extract the precise value of the slope of net baryon distribution in rapidity, at a fixed energy of the pp collision, or in semi-inclusive deep-inelastic scattering [26].
- We suggest to measure the energy and rapidity dependences of double baryon stopping in pp collisions. We expect that if the stopped baryons are close in rapidity, the rapidity distribution of the pair is flat [2].
- It will be useful to measure the rapidity distribution of $\bar{B}B$ pairs, as a function of rapidity separation between baryon and antibaryon. We expect that as a function of rapidity difference Δy between the baryon and antibaryon, the distribution will behave as $\exp(-0.82 \Delta y)$ at large Δy due to the J_0 exchange. The corresponding associated hadron multiplicity (per unit rapidity) in the rapidity interval Δy will be about 3/2 of the average multiplicity in inclusive events. At smaller Δy , J_2 and J_4 trajectories will contribute, and provide terms proportional to $\exp(-1.32 \Delta y)$ and $\exp(-1.74 \Delta y)$, with associated multiplicity densities that are about 1 and 1/2 of the inclusive multiplicity, correspondingly.
- It would be very important to measure the slope of the J_0 trajectory. One way of doing so is measuring the double-diffractive production of a baryon-antibaryon pair, as shown in Fig. 15. In a high-energy pp collision, this would amount to detecting a baryon and an antibaryon at mid-rapidity that are separated by rapidity gaps from both of the final-state protons (or their excited states). In this process, the JOZI rule will suppress the contribution of two Pomerons that usually dominate the double-diffractive processes, and enhance the Pomeron - J_0 fusion amplitude, see Fig. 15. Measuring the double differential cross section of this process would thus allow to extract the slope of the J_0 trajectory.
- Based on our prediction of degenerate \mathcal{C} -even and \mathcal{C} -odd J_0 trajectories we expect the existence of a heavy tensor $J^{PC} = 2^{++}$ $J\bar{J}$ glueball with mass $M \simeq 3.0 - 4.1$ GeV, which is heavier than the $M \simeq 2.4$ GeV tensor glueball measured on the lattice [23]. We also predict $J\bar{J}$ glueballs with $J^{PC} = 3^{-+}$ and $J^{PC} = 3^{--}$ with masses in the range 3.8 - 5.2 GeV. We suggest using correlations of junction-carrying lattice

operators, such as the one in (5.3), in order to enhance the sensitivity to these new states.

In conclusion, the phenomenon of baryon-number–flavor separation points to the fundamental role played by the string junction in transporting the baryon number. It is important to explore this fascinating QCD phenomenon further, both experimentally and theoretically.

Acknowledgments This work was supported in part by the U.S. Department of Energy, Office of Science, Office of Nuclear Physics, Grants No. DE-FG88ER41450 (DF, DK) and DE-SC0012704 (DK). GCR acknowledges partial financial support from INFN IS Lcd123.

A Derivation of equation (2.2)

In order to justify our starting point (2.2) it is better to begin, as in [3], from more differential (i.e. unintegrated) exclusive and inclusive cross sections and their generating functionals. This will also be useful to describe rapidity distributions, as well as flavor and baryon-number transport over large rapidity intervals. We shall then recover (2.2) upon integration over phase space.

We define the generating functional of exclusive cross sections by:

$$\Sigma[z(x)] = \sum_n \int \prod_{j=1}^n (dx^j z(x^j)) \frac{1}{\sigma_t} \frac{d\sigma(a+b \rightarrow x^1, x^2 \dots x^n)}{dx^1 dx^2 \dots dx^n} \quad (\text{A.1})$$

where x^j is a collective notation for the “coordinates” of the j^{th} final particle (i.e. whatever we want to measure about it: transverse momentum, rapidity, flavor, baryon number, etc.) and $d\sigma(x^1, x^2 \dots x^n)$ denotes the corresponding n -particle differential exclusive cross section, normalized to a suitably defined “total” cross section σ_t so that, by definition, $\Sigma[z(x) = 1] = 1$.

Clearly, individual exclusive differential cross section are given by partial functional differentiation of Σ evaluated at $z(x) = 0$. Instead, the m -particle inclusive cross section:

$$\rho_m(x^1, x^2 \dots x^m) = \frac{1}{\sigma_t} \sum_X \frac{d\sigma(a+b \rightarrow x^1, x^2 \dots x^m + X)}{dx^1 dx^2 \dots dx^m} \quad (\text{A.2})$$

is given by an order m functional differentiation of Σ evaluated at $z(x) = 1$.

A standard cluster-decomposition argument expresses those inclusive differential cross sections in terms of connected correlators defined via the expansion of:

$$\log \Sigma[z(x)] = \sum_m \frac{1}{m!} \int \prod_{j=1}^m [dx^j (z(x^j) - 1)] c_m(x^1, x^2 \dots x^m) \equiv p[z(x)]V \quad (\text{A.3})$$

around $z(x) = 1$. Σ , as defined in (A.1), is the analog of the grand-canonical partition function in statistical mechanics, whose logarithm is identified with $\frac{PV}{k_B T}$ after having taken a large- V thermodynamic limit.

In our context we may consider $k_B T$ to be fixed in terms of the average transverse momentum of the final particles while in (A.3) V is a fixed “volume factor” associated with the (log of the) total energy (see below) and $p[z(x)]$ plays the role of the pressure. Since we are interested in the high-energy limit, also in our case a large- V limit is understood. Indeed it is important to define $p[z(x)]$ as the coefficient of V in a large- V expansion of $\log \Sigma[z(x)]$ at fixed z . This implies that $p[z(x)]$ is insensitive to a V -independent (but possibly z -dependent) rescaling of Σ . For instance, one may like to add a z^{-2} overall factor in order to make Σ approach a finite limit for $z \rightarrow 0$, without affecting $p[z(x)]$.

The first few terms of the expansion give:

$$\begin{aligned}
\rho_1(x) &= c_1(x) \\
\rho_2(x^1, x^2) &= c_1(x^1)c_1(x^2) + c_2(x^1, x^2) \\
\rho_3(x^1, x^2, x^3) &= c_1(x^1)c_1(x^2)c_1(x^3) + c_2(x^1, x^2)c_1(x^3) + \text{perm.} + c_3(x^1, x^2, x^3) \\
\rho_4(x^1, x^2, x^3, x^4) &= c_1(x^1)c_1(x^2)c_1(x^3)c_1(x^4) + c_1(x^1)c_1(x^2)c_2(x^3, x^4) + \text{perm.} \\
&\quad + c_3(x^1, x^2, x^3)c_1(x^4) + \text{perm.} + c_2(x^1, x^2)c_2(x^3, x^4) + \text{perm.} + c_4(x^1, x^2, x^3, x^4) \dots \quad (\text{A.4})
\end{aligned}$$

Let us now comment on the relation between (A.4) and some equations in the main text. The first point is that, on the basis of a Mueller-Kancheli analysis [11, 12] one can argue that the correlators $c_m(x^1, x^2 \dots x^m)$ are short range in the sense that they fall off rapidly whenever any two subsets of the x^i get separated by a large distance in rapidity. Assuming also, that there is a finite transverse momentum cut off, integrating any c_m over its arguments will produce just single power of the total rapidity interval Y . This is to be contrasted with the integral of total correlators ρ_m which will typically grow as Y^m . So a term in the expansion (A.4) of ρ_m with a number q of connected correlators c will give a contribution of order Y^q (this is how the various contributions are ordered in (A.4)). The second observation is the well known fact (see e.g. [27]) that the total integral of ρ_m gives the expectation value $\langle n(n-1) \dots (n-m+1) \rangle$ explaining why we get such factors in the integrated form (2.2) of (A.4). We remark that the numerical coefficients appearing in (2.2) correspond exactly to the number of distinct permutations of each structure appearing in (A.4).

The extension of this procedure to the case of several species is rather straightforward and leads to results similar to those of (A.4). The main difference is that now we want to distinguish correlation within one species from correlation among different species. Then each term in the cluster decomposition will appear with the appropriate weight coming from the number of distinct ways to group the particles in separate clusters within and across different species.

References

- [1] G. C. Rossi and G. Veneziano, *A Possible Description of Baryon Dynamics in Dual and Gauge Theories*, *Nucl. Phys. B* **123** (1977) 507–545.
- [2] D. Kharzeev, *Can gluons trace baryon number?*, *Phys. Lett. B* **378** (1996) 238–246, [arXiv:nucl-th/9602027](https://arxiv.org/abs/nucl-th/9602027).

- [3] K. G. Wilson, *Some experiments on multiple production*, *CLNS-131* (11, 1970) .
- [4] G. Veneziano, *Large N Expansion in Dual Models*, *Phys. Lett. B* **52** (1974) 220–222.
- [5] G. Veneziano, *Some Aspects of a Unified Approach to Gauge, Dual and Gribov Theories*, *Nucl. Phys. B* **117** (1976) 519–545.
- [6] E. Witten, *Baryons and branes in anti-de Sitter space*, *JHEP* **07** (1998) 006, [arXiv:hep-th/9805112](#).
- [7] G. Rossi and G. Veneziano, *The string-junction picture of multiquark states: an update*, *JHEP* **06** (2016) 041, [arXiv:1603.05830 \[hep-th\]](#).
- [8] F. Bissey, F.-G. Cao, A. R. Kitson, A. I. Signal, D. B. Leinweber, B. G. Lasscock, and A. G. Williams, *Gluon flux-tube distribution and linear confinement in baryons*, *Phys. Rev. D* **76** (2007) 114512, [arXiv:hep-lat/0606016](#).
- [9] L. Montanet, G. C. Rossi, and G. Veneziano, *Baryonium Physics*, *Phys. Rept.* **63** (1980) 149–222.
- [10] S. M. Girvin and K. Yang, *Modern Condensed Matter Physics*. Cambridge University Press, 2019.
- [11] A. H. Mueller, *O(2,1) Analysis of Single Particle Spectra at High-energy*, *Phys. Rev. D* **2** (1970) 2963–2968.
- [12] O. V. Kancheli, *Inelastic differential cross sections at high energies and duality*, *JETP Lett.* **11** (1970) 267–270.
- [13] N. Lewis, W. Lv, M. A. Ross, C. Y. Tsang, J. D. Brandenburg, Z.-W. Lin, R. Ma, Z. Tang, P. Tribedy, and Z. Xu, *Search for baryon junctions in photonuclear processes and isobar collisions at RHIC*, [arXiv:2205.05685 \[hep-ph\]](#).
- [14] **Particle Data Group** Collaboration, R. L. Workman *et al.*, *Review of Particle Physics*, *PTEP* **2022** (2022) 083C01.
- [15] G. Veneziano, *Origin and intercept of the Pomeranchuk singularity*, *Phys. Lett. B* **43** (1973) 413–416.
- [16] R. P. Feynman, *Very high-energy collisions of hadrons*, *Phys. Rev. Lett.* **23** (1969) 1415–1417.
- [17] R. P. Feynman, *The behavior of hadron collisions at extreme energies*, *Conf. Proc. C, 3rd International Conference on High Energy Collisions, 5-6 September 1969, Stony Brook, NY* (1969) 237–258.
- [18] D. Amati, A. Stanghellini, and S. Fubini, *Theory of high-energy scattering and multiple production*, *Nuovo Cim.* **26** (1962) 896–954.
- [19] K. G. Wilson, *Regge poles and multiple production*, *Acta Phys. Austriaca* **17** (1963) 37–44.
- [20] G. 't Hooft, *A Planar Diagram Theory for Strong Interactions*, *Nucl. Phys. B* **72** (1974) 461.
- [21] G. F. Chew and A. Pignotti, *Multiperipheral bootstrap model*, *Phys. Rev.* **176** (1968) 2112–2119.
- [22] H. Lee, *How to generate the Pomeranchukon from the background in a dual multiperipheral model*, *Phys. Rev. Lett.* **30** (1973) 719–722.
- [23] Y. Chen *et al.*, *Glueball spectrum and matrix elements on anisotropic lattices*, *Phys. Rev. D* **73** (2006) 014516, [arXiv:hep-lat/0510074](#).

- [24] **Particle Data Group** Collaboration, K. A. Olive *et al.*, *Review of Particle Physics*, *Chin. Phys. C* **38** (2014) 090001.
- [25] V. A. Novikov, L. B. Okun, M. A. Shifman, A. I. Vainshtein, M. B. Voloshin, and V. I. Zakharov, *Charmonium and Gluons: Basic Experimental Facts and Theoretical Introduction*, *Phys. Rept.* **41** (1978) 1–133.
- [26] D. Frenklakh, D. E. Kharzeev, and W. Li, *Signatures of baryon junctions in semi-inclusive deep inelastic scattering*, *Phys. Lett. B* **853** (2024) 138680, [arXiv:2312.15039 \[hep-ph\]](#).
- [27] C. E. DeTar, D. Z. Freedman, and G. Veneziano, *Sum rules for inclusive cross-sections*, *Phys. Rev. D* **4** (1971) 906–909.